ELSEVIER

Journal of Nuclear Materials 266–269 (1999) 399–405

journal of nuclear materials

Chemical erosion of graphite under simultaneous O^+ and H^+ irradiation

Allen Y.K. Chen *, J.W. Davis, A.A. Haasz

Fusion Research Group, University of Toronto Institute for Aerospace Studies, 4925 Dufferin Street, Toronto Ont., Canada M3H 5T6

Abstract

Our present investigation of the chemical erosion of graphite during simultaneous O^+ and H^+ irradiation was undertaken to gain an understanding of the reaction mechanisms, by varying the implantation depth and the incident flux ratio (Φ_O/Φ_H) of the two ion species. The results indicate that the yields of CO and CO_2 are reduced when H^+ is added to O^+ irradiation whereas the yield of CH_4 is reduced when O^+ is added to H^+ irradiation. Furthermore, these reductions are accompanied by the formation of H_2O. We found that the relative ion range has negligible effect on the H_2O yield, as well as on the reduction of CO, CO_2 and CH_4 formation during O–H–C reactions as compared to O–C reactions (CO and CO_2) and H–C reaction (CH_4). The relative changes of CO, CO_2, and CH_4 yields, as well as H_2O production, however, do depend on flux ratio. The reductions of CO/O^+ and CO_2/O^+ yields during H^+ and O^+ co-bombardment are highest for 'small' Φ_O/Φ_H flux ratios; the corresponding water production is also highest for Φ_O/Φ_H flux ratios. On the other hand, the reductions of CH_4/H^+ yields during H^+ and O^+ co-bombardment, as compared to H–C reactions, are highest for 'large' Φ_O/Φ_H flux ratios. A plausible mechanism is proposed to explain the observed synergistic effects.

Keywords: Carbon; Chemical erosion; Graphite; Hydrogen; Oxygen; Ion bombardment

1. Introduction

Graphite is one of the prime candidates for first-wall use in fusion devices. It has excellent thermomechanical properties enabling it to withstand the high-power flux inside fusion reactors, and its low-Z reduces the effects of fuel dilution and plasma cooling. Unfortunately, in addition to normal physical sputtering, graphite is susceptible to chemical attack. Exposure to hydrogen – the fusion fuel – in the temperature range 300–1000 K leads to the formation of volatile hydrocarbons. Furthermore, since oxygen is often the main intrinsic impurity in the plasma of current fusion devices with carbon walls, the reaction of oxygen-containing ions with carbon materials also plays an important role in the complex process of plasma wall interaction. Carbon erosion due to separate bombardment by H^+ and O^+ has been studied extensively [1,2], but only limited data exist currently on the effect of exposing graphite simultaneously to energetic oxygen and hydrogen [2,3]. Our previous investigation of the temperature dependence of chemical erosion yields [3] has demonstrated the formation of water molecules and small reductions of both the CO and CO_2 yields during simultaneous H^+ and O^+ bombardment. The present study attempts to uncover further details of the mechanisms of the interaction between the oxygen ions and hydrogen ions in the carbon system by varying the energies (i.e., the implantation depth) and fluxes of the two ion beams.

2. Experimental setup

The erosion of graphite has been studied under conditions of simultaneous bombardment by O_2^+ and H_3^+ ions, using an independently controlled high-flux, low-energy, mass-analyzed dual-beam ion accelerator system [4]. The hydrogen ions were produced from a

* Corresponding author. Tel.: +1 416 667 7891; fax: +1 416 667 7799; e-mail: allen@starfire.utias.utoronto.ca

0022-3115/99/$ – see front matter
PII: S0022-3115(98)00514-5

pure hydrogen gas by a duoplasmatron ion source with a hot filament cathode coated with a barium-containing compound. The oxygen ions were produced from a 10%-oxygen/90%-helium gas mixture by a modified duoplasmatron ion source fitted with a stainless steel hollow cathode. From previous studies of methane formation from graphite under energetic H^+ and H_3^+ irradiation, the H_3^+ molecular ions were found to behave effectively as three H^+ ions with one-third of the H_3^+ ion energy [5]. Thus, it is assumed that the incident O_2^+ and H_3^+ molecular ions break up immediately into atoms upon impact with the specimen, and act independently within the graphite.

The two beams intersected in the target chamber with a 42° angle of separation, and the target specimen was normally placed at the point of intersection such that the beams were 21° from the surface normal; see Fig. 1. Beam energies were in the ranges 0.7–3 keV/H^+ and 2.5–5 keV/O^+, with the energy ratio (E_O/E_H) being in the range ~0.8–7.1. The depth profiles (Fig. 2) of both O^+ and H^+ beams, based on the energies used and a target density of 2200 kg/m^3, were calculated using the TRVMC program [6]. Beam fluxes were in the range ~2.5–4.8 × 10^{19} H^+/m^2 s and ~0.3–1.8 × 10^{19} O^+/m^2 s, with the flux ratio (Φ_O/Φ_H) being in the range ~10–50%. (Here we use H^+ and O^+ to designate incident particles, even though not all of the atoms in the H_3^+ and O_2^+ molecular ions are charged.) The beam spots, slightly elliptical in shape due to off-normal incidence, were ~5 mm (for H^+) and ~3 mm (for O^+) in diameter. This allowed complete overlapping of the O^+ beam spot by the H^+ spot at the focus.

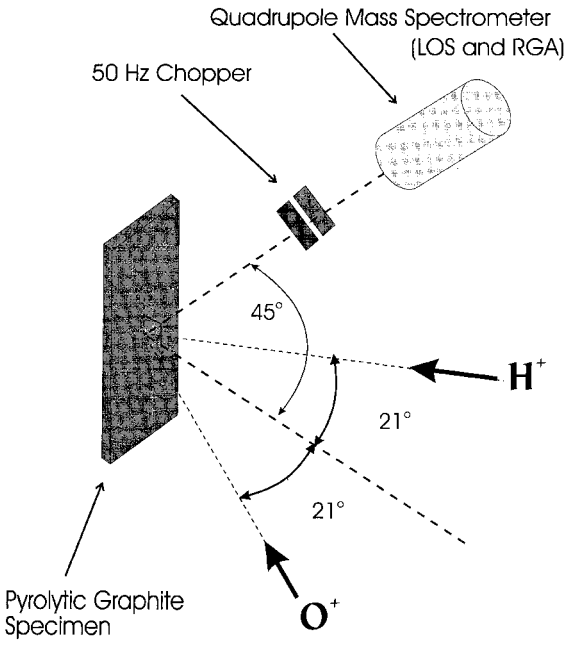

Fig. 1. Schematic diagram of the apparatus configuration in the vacuum chamber.

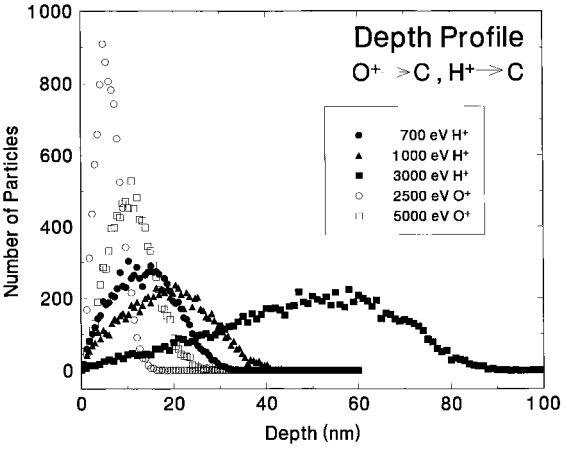

Fig. 2. Implantation depth profiles for H^+ and O^+ in amorphous graphite calculated for an incidence angle of 21° by the TRVMC [6] program.

The specimen was a strip of 'as-deposited' pyrolytic graphite (HPG99 from Union Carbide) with a density of ~2200 kg/m^3, a mosaic spread of ~30°, and approximate dimensions of 30 × 10 × 0.5 mm^3 with uniform thickness throughout the specimen. It was held by stainless steel jaws to allow direct current heating, and was biased at +30 V to suppress secondary electrons. The temperature dependence behaviour of the erosion yields, from previous experiments with relatively fixed energy and flux ratios, indicate that the greatest synergistic effects occur at a specimen temperature of ~800 K [3]. Therefore, for the present energy and flux-ratio dependence experiments, the specimen temperature was fixed at ~800 K; the temperature was monitored with an optical pyrometer.

The target chamber in which the specimen was housed was baked for at least 24 h at ~500 K before the experiments. The specimen was heated to >1250 K for several hours in order to eliminate intrinsic H and O impurities. Reaction products were measured by quadrupole mass spectrometry (QMS) in both residual gas analysis (RGA) and line-of-sight (LOS) modes, all in steady state. Typical pressure in the target chamber during the experiments was about 10^{-5} Pa consisting mainly of He and H_2 from the ion sources. A computer controlled data acquisition system was used to collect QMS data.

The absolute erosion yields of methane, carbon monoxide and carbon dioxide were obtained by using commercially produced calibrated leaks with an absolute error of 20%. The absolute value of the water production rate (in O–H–C reactions) was estimated on the

basis of the reduction of the CO/O^+ and CO_2/O^+ yields during H^+ and O^+ co-bombardment (i.e., via the oxygen balance method).

3. Results and analysis

For each depth-ratio and flux-ratio combination, the experiment consisted of four phases: (I) O^+ irradiation only, (II) simultaneous O^+ and H^+ irradiation, (III) H^+ irradiation only, and (IV) no irradiation. Fig. 3 shows a typical experimental raw signal trace at ~800 K in the RGA mode. The CO, CO_2, and H_2O yields corresponding to simultaneous O^+ and H^+ exposures were obtained from the differences between the phases II and III signals, the latter being the effective background (mainly from H^+-included signals coming from the chamber walls, etc.). Similarly, the CO and CO_2 yields corresponding to O^+-only exposure were obtained from the differences between the phases I and IV signals, the latter being the background signal with no beams on. The water yield during O^+-only exposure is insignificant and is discarded, as we are only interested in the water produced during O–H–C reactions. For the evaluation of the CH_4 yield, the yield that corresponds to simultaneous O^+ and H^+ exposure was obtained from the difference between the phases II and I signals, the latter being the effective background (mainly from O^+-induced CH_4 signal from chamber surfaces which was found to be negligible). The CH_4 yield that corresponds to H^+-only exposure was obtained from the difference between the phases III and IV signals. All of the signals discussed above, except for water, were then calibrated against respective absolute leaks to obtain absolute yield values. Details of the calculations can be found in Ref. [3].

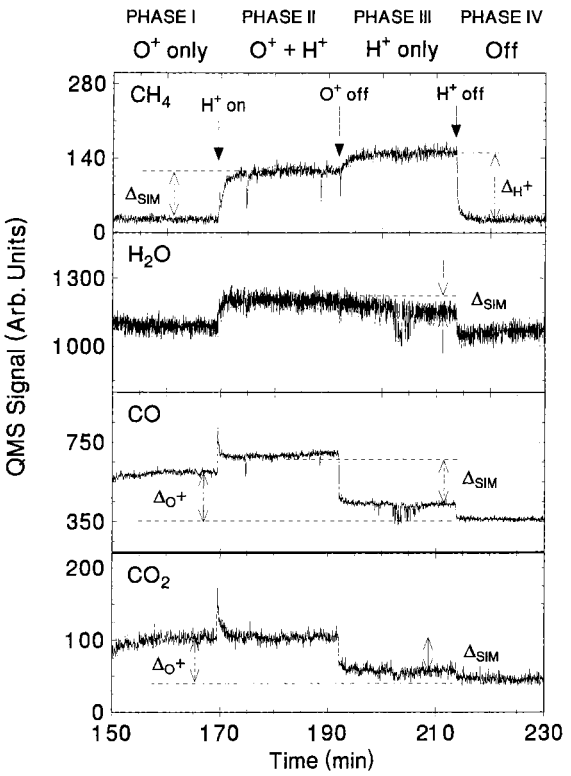

Fig. 3. Typical raw traces of the QMS signals of H_2O, CO, CO_2, and CH_4 in the RGA detection mode during 5 keV O^+ and 700 eV H^+ bombardment of graphite at 800 K. The flux ratio Φ_O/Φ_H is ~0.3. The traces are divided into four phases: (I) O^+ beam only: (II) simultaneous O^+ and H^+ irradiation; (III) H^+ beam only; and (IV) both beams turned off. Δ_O^+ is the QMS signal for CO, CO_2 and H_2O due to O^+-only bombardment; Δ_H^+ is the QMS signal for CH_4 due to H^+-only bombardment; and Δ_{SIM} is the QMS signal due to O^+ and H^+ co-bombardment.

The data reduction method described here also effectively subtracts contributions from any O_2(gas)–ion–C and H_2(gas)–ion–C interactions (here 'ion' refers to either H^+ or O^+). We further note that at 800 K, contributions from O_2 and H_2 are expected to be very small. It is known that H_2 and O_2 gas molecules do not react significantly with carbon at 800 K [2]. However, in order to get an upper limit of the effect of O_2 on the measured signals in the presence of ion irradiation, we use published erosion yields for the O_2–Ar^+(5 keV)–C reaction at 800 K: $\sim 10^{-3}$ CO/O_2 and $\sim 10^{-4}$ CO_2/O_2 [2]. We expect the erosion enhancement due to Ar^+ (5 keV) to be at least as large as, and perhaps larger than, the enhancement due to H^+ ($\leqslant 3$ keV) and/or O^+ ($\leqslant 5$ keV). With our O_2 background partial pressure of $\sim 3\times 10^{-7}$ Pa, the CO contribution to our QMS signal from the O_2–ion–C reaction at 800 K is expected to be about 5 orders of magnitude smaller than that obtained from the O^+–C reaction, taking into account the differences in flux densities and reaction yields. In the case of H_2–O^+–C reaction, it is evident from the CH_4 trace in Fig. 4 that the contribution of H_2 to the QMS signal is negligible (compare phases I and IV, the latter being the background). Furthermore, since H^+ is much less massive than O^+, we also expect negligible contribution to the QMS signals in the H_2–H^+–C reaction cases.

Note the O^+-induced wall effects for the CO and CO_2 signals and the H^+-induced wall effects for the CH_4 signals cannot be eliminated using the above method. For this reason we performed identical experiments for a few selected cases in the LOS mode, in which the background effects are manifested as noise instead of a signal shift. Absolute calibration of the LOS signals was not possible in our current experimental setup. However, by calculating the *fraction* of the yield reduction of the O–H–C reactions with respect to the O–C reactions, and matching this fraction to the corresponding RGA results, we were able to determine the contribution of wall effects to the RGA results for CO and CO_2. LOS experiments also show that the water signal drop during

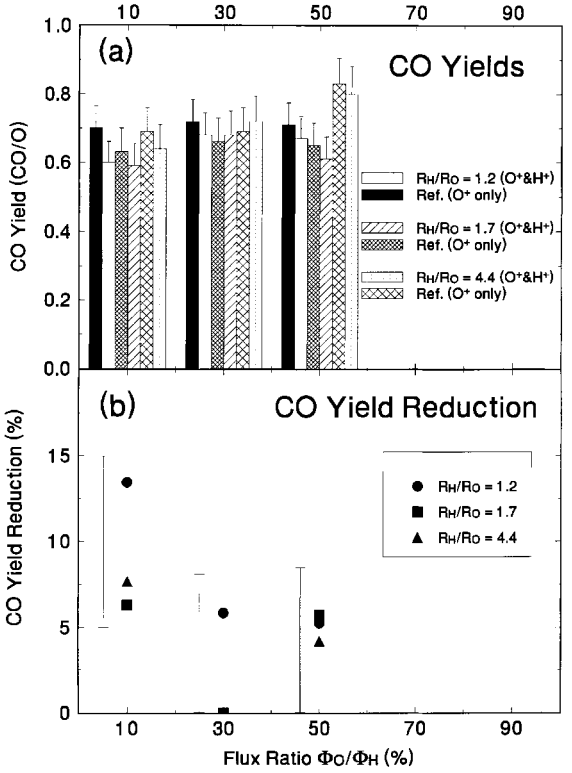

Fig. 4. (a) CO yields, as measured by RGA, as a function of flux ratio Φ_O/Φ_H for various implantation depth ratios R_H/R_O. Yields from both the O^+–only irradiation and O^+ and H^+ co-bombardment cases are shown. (b) CO yield reduction, in percentage, as a function of flux ratio Φ_O/Φ_H for the implantations shown in (a).

transition between phases II and III is equally sharp as those from other species. The corresponding slower drop observed during RGA experiments (see Fig. 3) is mainly due to the much lower effective water pumping speed, which is caused by water molecules attaching to wall surfaces in the target chamber.

To ensure that the contribution of the O^+-induced background effects is relatively small and constant for ease of analysis, we have selected from our results for analysis and presentation only those cases with a fixed O^+ flux (3×10^{18} O^+/m^2 s), and a fixed O^+ energy (5 keV). From the calculated depth profiles shown in Fig. 2, it is evident that the O^+-implantation depth is much shallower and localized than the depth for H^+. Hence, limiting the O^+ beam to a fixed energy simplifies the analysis and interpretation of the results. We are, however, able to freely vary the energy and flux of the H^+ beam since the wall effect produced in phase III of the experiments is always subtracted for CO and CO_2 analysis. Furthermore, previous experiences also indicate that the H^+-induced background effect for CH_4 production with H^+ ions in the energy range used here (0.7–3 keV/H^+) is negligible. This is confirmed by the comparison between the LOS and RGA results in the manner described above. The O^+-induced wall contribution also turns out to be negligible in the case of CO. For CO_2, however, the O^+-induced background effect is ~0.04 CO_2/ O^+, or 20–40% of the measured RGA signals.

The RGA results, after the above analysis, are shown in Figs. 4–7 for CO, CO_2, CH_4 and H_2O, respectively. The (a) parts of Figs. 4–6 show the yields for three different implantation *depth ratios* ($R_H/R_O = 1.2$, 1.7, 4.4) plotted against the flux ratio. Yields from both dual-beam and single-beam reactions are plotted for CO (Fig. 4), CO_2 (Fig. 5), and CH_4 (Fig. 6), but water production is only plotted (Fig. 7) for the O–H–C reactions. The single beam yields are plotted for reference; variations in these yields indicate the *run-to-run* uncertainties in the measurement. (We note that typically one or two runs were performed in a day.) The error bars indicate the actual signal variations within a *specific run* of a particular depth-ratio and flux-ratio combination.

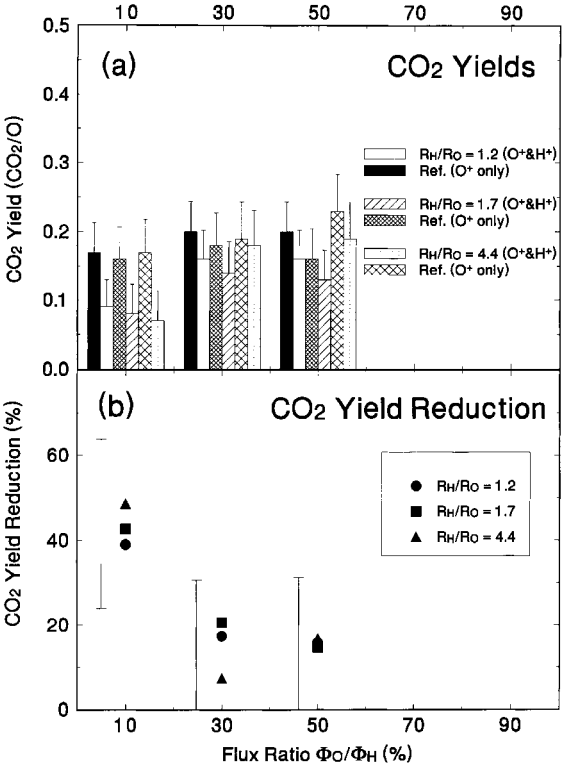

Fig. 5. (a) CO_2 yields, as measured by RGA, as a function of flux ratio Φ_O/Φ_H for various implantation depth ratios R_H/R_O. Yields from both the O^+-only irradiation and O^+ and H^+ co-bombardment cases are shown. (b) CO_2 yield reduction, in percentage, as a function of flux ratio Φ_O/Φ_H for the implantations shown in (a).

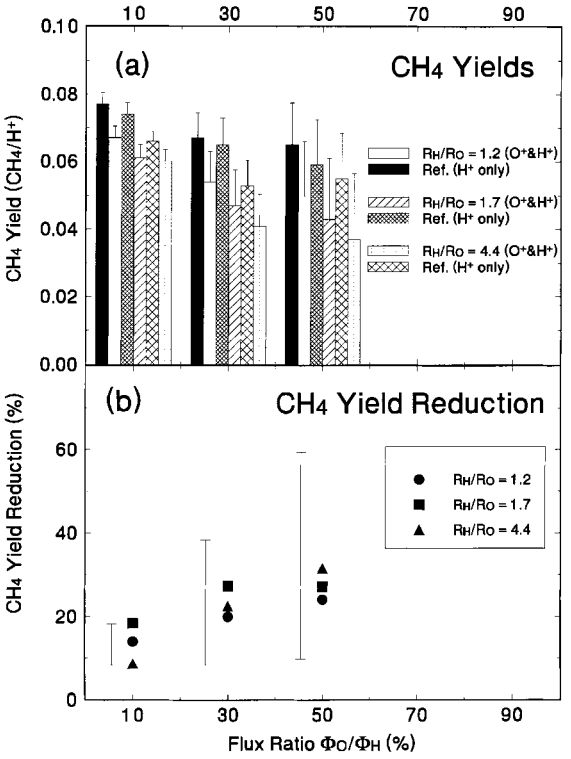

Fig. 6. (a) CH_4 yields, as measured by RGA, as a function of flux ratio Φ_O/Φ_H for various implantation depth ratios R_H/R_O. Yields from both the H^+-only irradiation and O^+ and H^+ co-bombardment cases are shown. (b) CH_4 yield reduction, in percentage, as a function of flux ratio Φ_O/Φ_H for the implantations shown in (a).

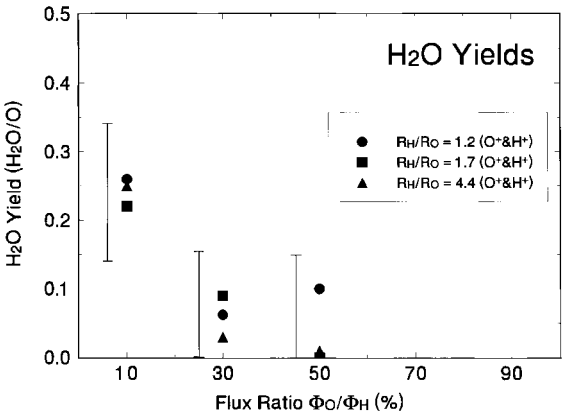

Fig. 7. H_2O yields, as measured by RGA, plotted as a function of flux ratio Φ_O/Φ_H for various implantation depth ratios R_H/R_O. Yields are shown only for the O^+ and H^+ co-bombardment cases.

The CO, CO_2 and CH_4 yields drop during H^+ and O^+ co-bombardment, in comparison with the respective single species irradiation cases. These drops are accompanied by the formation of H_2O. As the time span for QMS data measurements from the single-beam and simultaneous irradiation phases of a *particular run* was about an hour or so, the run-to-run uncertainties are not expected to affect the analysis of the *yield reduction* and *water formation* derived from a *particular run*.

The percentage reductions of the CO, CO_2 and CH_4 yields in O–H–C reactions, as compared with O–C reactions (in the cases of CO and CO_2) and H–C reactions (in the case of CH_4), are plotted separately in the (b) parts of Figs. 4–6, again as a function of flux ratios. A depth (or range) ratio (R_H/R_O) of ~1.2 indicates a near-complete overlapping (as estimated by the TRVMC program; see Fig. 2) of the O^+ and H^+ ion ranges. On the other hand, a depth ratio of ~4.4 indicates a complete separation of O^+ and H^+ implantation; the estimated ranges (Fig. 2) for the 5 keV O^+ and the 3 keV H^+ are ~11 and ~50 nm, respectively. It is evident that within the uncertainty of the data, the depth ratio has no effect on the reductions of CO and CO_2 yields during O–H–C reactions when compared to the O–C reactions, and on the reduction of CH_4 yields during O–H–C reactions when compared to the H–C reactions. Water production is also not significantly affected by the depth ratio; see Fig. 7.

The yield changes, however, do depend on the incident ion flux ratio. The reductions of CO yields range from ~10% (for $\Phi_O/\Phi_H = 0.1$) to ~5% (for $\Phi_O/\Phi_H = 0.3$–0.5), and roughly similar for all depth ratios. The reductions of CO_2 yields range from ~45% (for $\Phi_O/\Phi_H = 0.1$) to ~15% (for $\Phi_O/\Phi_H = 0.3$–0.5), and again similar for all depth ratios. Reductions of the CH_4 yields range from ~15% (for $\Phi_O/\Phi_H = 0.1$) to ~30% (for $\Phi_O/\Phi_H = 0.5$). A calibration for the H_2O yields was estimated using the oxygen balance method from the CO and CO_2 reductions for the case of 10% Φ_O/Φ_H flux ratio with complete ion-range overlap. All other cases were calculated relative to this value. Thus we found water production to be about 0.25 H_2O/O^+ for $\Phi_O/\Phi_H = 0.1$, dropping to below 0.1 H_2O/O^+ for larger flux ratios.

4. Discussion

We proceed to examine the physical mechanisms of the synergistic effect of simultaneous O^+ and H^+ irradiation and the resulting water production. See Fig. 8 for an illustration of the mechanisms discussed below. From our experiments, we note that H_2O production and the reduction of the other species are not dependent on the depth ratio R_H/R_O. We propose the hypothesis that for the O–C case, all the oxygen participates in the reactions with carbon to form CO and CO_2 at the end of the O^+ ion range, since we and others [7] do not observe the release of any O_2. Also, our oxygen balance for the O–C reactions is nearly unity [3]. This suggests that there

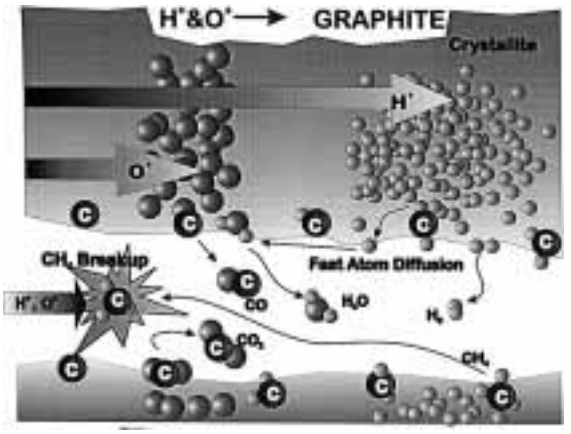

Fig. 8. An illustration of the reaction mechanisms representing the case of total implantation depth separation of simultaneous O^+ and H^+ implantation. Here, mobile hydrogen atoms undergo fast atom diffusion via internal surfaces of intercrystalline paths (represented by the white channel) and either recombine to form H_2 molecules or react with oxygen on the internal surfaces to form H_2O molecules. This process competes with the localized O–C reactions and limits the production of CO and CO_2 molecules. Meanwhile, CH_4 molecules formed at the end of the H^+ ion-range also move freely via the internal channel, but are broken up by incident H^+ and O^+ ions. This also limits the production of CH_4 even though the C–H reactions are not directly involved with O^+ because of the range separation.

are no free O atoms that are mobile within the carbon matrix to form O_2 via recombination, or more importantly, in the case of O^+ and H^+ co-bombardment, to react with hydrogen elsewhere to form water molecules. On the other hand, previous hydrogen isotope-mixing experiments show that some mobile H-atoms freely move through intercrystalline channels, or internal porosity, within the ion-range [8–10]. Thus, during simultaneous H^+ and O^+ irradiation, the hydrogen atoms can readily react with oxygen even when the end of ion range for H^+ is much larger than that of O^+. The reaction of hydrogen with available oxygen takes away a portion of the oxygen supply, resulting in the observed reductions of CO and CO_2 yields, compared to the O–C reaction case.

We also observe from our results that the yields depend on the flux ratio. The smaller the oxygen flux compared to the hydrogen flux, the greater is the reduction of CO and CO_2 yields, and the greater is the H_2O yield. This might be explained by noting that when there is an over-abundance of available hydrogen, such as in the case when Φ_O/Φ_H is relatively low (e.g., $\Phi_O/\Phi_H \sim 0.1$), relatively more hydrogen can go into the production of H_2O. We also observe that the reduction of CO_2 is much higher than that of CO when there is an over-abundance of available hydrogen. This can be explained by noting that since it takes twice as many oxygen atoms to form one CO_2 molecule than one CO, when the oxygen supply is reduced due to H_2O formation, it would show a greater effect on CO_2 production than on CO production.

The behaviour of CH_4 shows the opposite effect in its flux-ratio dependency: at a low Φ_O/Φ_H flux ratio, the synergistic reduction of the CH_4 production is smaller than that seen for the higher flux ratios. Previous studies indicate that the production of methane occurs at the end of the H^+ ion range and that the methane molecules move through the internal porosity to be released from the surface [9–14]. This suggests that in the simultaneous O–H–C reactions, methane production is not directly involved with CO and CO_2 productions when the two ion ranges are completely separated (O atoms do not diffuse). The reduction of CH_4 in this case comes entirely from a previously observed phenomenon known as "methane break-up" where methane molecules are formed at the end of ion range, and while moving towards the surface via internal porosity they undergo fragmentation by incident ions [15,16]. This effect is expected to increase with the addition of energetic O^+ ions. Furthermore, when more energetic oxygen ions are present in the system relative to hydrogen ions, as in the case for the highest flux ratio (i.e. $\Phi_O/\Phi_H = 0.5$), methane break-up increases and we see a larger steady state CH_4 reduction. The break-up effect might also be expected to be seen in the release of CO_2 and H_2O, but we suspect that the effect is much less pronounced than it is on CH_4 . This is because the reactions that form CO_2 and H_2O take place much closer to the surface, thus the molecules are less likely to encounter the incident ions during their transport out of the graphite. For the case where the two ion ranges are overlapping, we cannot at this time separate the contributions of methane break-up and water-formation to the observed methane reduction.

The intense ion bombardment employed in the current experiments will lead to the formation of a complex surface morphology. Although the surface does become amorphous, it does retain some of the microcrystalline structure [17]. The associated variations in the microstructure of the surface may well affect the relative H^+ and O^+ ranges. Assuming as the original specimen, $\pm 30°$, relative ranges will not be greatly affected (based on TRVMC calculations of $21 \pm 30°$). This assumption is not totally unreasonable since the two beams incident at off-normal angles are expected to prevent the formation of any major surface features. Furthermore, the surface recession that occurs due to erosion also does not affect the reactions. As the target temperature in the present study is fixed at 800 K, almost no H trapping occurs at the end of the ion range. Therefore, all reactions are with dynamic or solute H, and reaction of the surface will have no impact on the relative placement of solute H and the O^+ range. It is possible, however, that

for ion-range separation experiments performed at lower temperatures, the location of trapped H could be affected by surface recession, and this may have an impact on the erosion chemistry.

5. Summary

We have presented results of further studies of the synergistic interaction occurring during simultaneous H^+ and O^+ irradiation of graphite. We have concentrated on the effect of varying the *ion range ratio* and *flux ratio* of the two impacting ion species. The results indicate that the range ratio has negligible effect on H_2O formation and the reductions of CO and CO_2 yields during O–H–C reactions, as compared to O–C reactions; also, negligible effect is seen on the reductions of CH_4 yields during O–H–C reactions, as compared to H–C reactions. The reactions, however, do depend on the flux ratio Φ_O/Φ_H. The reduction of CO/O^+ yields during H^+ and O^+ co-bombardment decreases from ~10% (for $\Phi_O/\Phi_H = 0.1$) to ~5% (for $\Phi_O/\Phi_H = 0.3$–0.5). The corresponding reductions of CO_2/O^+ yields are ~45% and ~15%, respectively. Water production drops from roughly 0.25 H_2O/O^+ for $\Phi_O/\Phi_H = 0.1$ to below 0.1 H_2O/O^+ for higher flux ratios. Reductions in the CH_4/H^+ yield were in the range 15–30%, increasing with the flux ratio Φ_O/Φ_H. We propose the hypothesis that H_2O formation occurs at the end of the O^+ ion range. This is consistent with the observed effect that H_2O yields and reductions of CO and CO_2 yields are independent of the O^+ and H^+ range separation.

Acknowledgements

This work was supported by the Canadian Fusion Fuels Technology Project and the Natural Sciences and Engineering Research Council of Canada. We thank Dr. W. Eckstein of IPP Garching for providing us the TRVMC code. Thanks are also extended to Charles Perez for his help with the preparation of the apparatus. We also gratefully acknowledge discussion with Dr. E. Vietzke of the KFA Forschungszentrum, Jülich, that led to the modification (installation of hollow cathode) of our duoplasmatron ion source for stable oxygen beam operation.

References

[1] W. Eckstein, V. Philipps, in: W.O. Hofer, J. Roth (Eds.), Physical Processes of the Interaction of Fusion Plasmas with Solids, Academic Press, Amsterdam, 1996, p. 93.
[2] E. Vietzke, A.A. Haasz, in: W.O. Hofer, J. Roth (Eds.), Physical Processes of the Interaction of Fusion Plasmas with Solids, Academic Press, Amsterdam, 1996, p. 135.
[3] A.A. Haasz, A.Y.K. Chen, J.W. Davis, E. Vietzke, J. Nucl. Mater. 248 (1997) 19.
[4] A.A. Haasz, J.W. Davis, Nucl. Instrum. and Meth. B 83 (1993) 117.
[5] A.A. Haasz, J.W. Davis, O. Auciello, P.C. Stangeby, E. Vietzke, K. Flaskamp, V. Philipps, J. Nucl. Mater. 145–147 (1987) 412.
[6] W. Eckstein, TRVMC: Vectorized TRIM code for Sputtering, Multi-Component, IPP Garching, FRG, 1993.
[7] E. Vietzke, T. Tanabe, V. Philipps, M. Erdweg, K. Flaskamp, J. Nucl. Mater. 145–147 (1987) 425.
[8] S. Chiu, A.A. Haasz, J. Nucl. Mater. 210 (1994) 34.
[9] S. Chiu, A.A. Haasz, J. Nucl. Mater. 196–198 (1992) 972.
[10] A.A. Haasz, P. Franzen, J.W. Davis, S. Chiu, C.S. Pitcher, J. Appl. Phys. 77 (1995) 66.
[11] V. Philipps, K. Flaskamp, E. Vietzke, J. Nucl. Mater. 128&129 (1984) 545.
[12] J. Roth, J. Bohdansky, Appl. Phys. Lett. 51 (1987) 964.
[13] R. Yamada, J. Appl. Phys. 67 (1990) 4118.
[14] S. Chiu, A.A. Haasz, J. Nucl. Mater. 208 (1994) 282.
[15] S. Chiu, A.A. Haasz, P. Franzen, J. Nucl. Mater. 218 (1995) 319.
[16] A.A. Haasz, S. Chiu, P. Franzen, J. Nucl. Mater. 220–222 (1995) 815.
[17] W. Möller, J. Nucl. Mater. 162–164 (1989) 138.